Combining Immunolabeling and Surface-Enhanced Raman Spectroscopy on Cell Membranes

Matthew D. Hodges,[†] Jemma G. Kelly,[‡] Adam J. Bentley,[†] Simon Fogarty,[†] Imran I. Patel,[‡] Francis L. Martin,[‡] and Nigel J. Fullwood[†,*]

[†]Division of Biomedical and Life Sciences, School of Health and Medicine, Lancaster University, Lancaster, United Kingdom, LA1 4YQ, and [‡]Centre for Biophotonics, Lancaster Environment Centre, Lancaster University, Lancaster, United Kingdom, LA1 4YQ

ABSTRACT

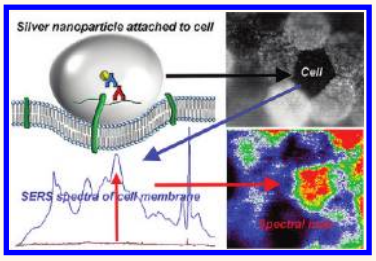

We applied surface-enhanced Raman spectroscopy (SERS) to immunolabeled endothelial cells to derive enhanced spectra of the biomolecular makeup of the cellular surface. A two-step immunolabeling protocol with gold-conjugated antibodies coupled with silver enhancement to attach silver nanoparticles to the cell surface was employed. This approach generated ~50-fold SERS enhancement of spectral signals. The SERS spectra exhibited several SERS-enhanced peaks associated with cell membrane components. The SERS detection of silver nanoparticles proved more far more sensitive than conventional light microscopy techniques. The SERS enhancement allowed us to carry out spectral mapping using wavenumbers associated with membrane components that correlated directly with the distribution of silver nanoparticles. SERS has the potential to detect immunolabeling at lower levels than is possible using conventional immunolabeling methods while simultaneously providing unique, spatially defined, biochemical information.

KEYWORDS: cell membrane · surfaced-enhanced Raman · silver nanoparticles · immunolabeling · keratan sulfate · lipids · proteins

The use of immunological antibodies conjugated to colloidal gold particles for the detection of specific epitopes has been used for several decades in both light and electron microscopy.[1] This technology allows the direct visualization of the gold nanoparticles, typically 5–20 nm in size, with the transmission electron microscope (TEM). For visualization with the light or scanning electron microscope (SEM), a silver enhancement procedure is used. This involves using the gold nanoparticles as nuclei to reduce silver ions in the silver-enhancing solution to metallic silver particles. The size of the silver particles can be controlled by varying the duration of the enhancement procedure. This technology is now used for the detection of epitopes with applications in immunohistochemistry, immunoblotting, and immunoassay techniques.[2–4]

Metallic nanoparticles are also extensively used in spectroscopy, particularly in the emerging field of biospectroscopy. The application of spectroscopy technology to the field of biomedicine is a fast-moving field of research.[5] Unlike immunolabeling and immunoassay techniques, which provide information on a single biomolecule within a cell, spectroscopy has the potential to simultaneously detect all classes of biomolecules, including proteins, lipids, carbohydrates, and nucleic acids.[6] Gold and silver nanoparticles can be used in Raman spectroscopy to enhance the spectral signal from biological samples.[7] This technique, surface-enhanced Raman spectroscopy (SERS), is one of the most exciting areas in spectroscopy today. It is known that this can occur either with electromagnetic enhancement dependent upon the excitation of plasmons from the metal[8] or *via* chemical enhancement if the molecule forms bonds with the metal surface. The degrees of enhancement can be influenced by many factors,[9] including the presence of dimers,[10,11] the shape and size of the nanoparticles,[12–15] the density of nanoparticles,[16] and the proximity of adjacent nanoparticles.[17] The excitation wavelength is also a critical factor.[15] Under optimum conditions, the signal may be amplified by many orders with enhancements in the range of 10^8 to 10^{15} magnitudes.[18]

Most of the work on SERS uses nanoparticles conjugated to reporter molecules, which results in an enhanced signal for the reporter molecule attached to the nanoparticle. This is an extremely powerful and sensitive

* Address correspondence to n.fullwood@lancaster.ac.uk.

Received for review July 15, 2011 and accepted November 8, 2011.

Published online November 08, 2011
10.1021/nn202652h

technique and has a wide and increasing number of applications in the biomedical field. However, it is also possible to use metallic nanoparticles without reporter molecules, in which case the enhanced Raman signal can be obtained from the immediate locality surrounding the nanoparticle. The distance away from the nanoparticle that the majority of the enhanced signal is produced has been estimated to be ~15 nm.[19] This is of particular interest to biomedical researchers because this technique has the potential to provide information on all of the biomolecules in the immediate locality of the nanoparticle, *e.g.*, the molecular composition of the cell surface. This is information that is difficult to obtain in any other way. To many biomedical researchers, SERS spectroscopy is seen as an exotic and difficult technique, with no direct relevance to their work. This is despite the fact that almost every biomedical researcher will use some form of immunolabeling or immunoassay technique as a routine part of their work with many employing the gold/silver enhancement technique.

This paper combines two important technologies, the established one of colloidal gold immunolabeling and silver enhancement and the newly emerging one of SERS spectroscopy. We had two objectives: first, to determine whether cell labeling using conventional immunogold labeling and silver enhancement techniques could be used to enhance the biomolecular Raman spectra from cell surfaces. Our second objective was to determine if SERS was capable of detecting the silver nanoparticles on immunolabeled cells at a higher sensitivity than conventional methods. Specifically, we wanted to compare the sensitivity of SERS for detecting antibody-conjugated nanoparticles with that of conventional light microscope-based methods.

In this paper, we used a model system, the corneal endothelium. The corneal endothelial cells form a monolayer on Descemet's membrane on the inner surface of the cornea where the apical surface of the endothelial cells is readily accessible for antibody labeling. In addition, the corneal endothelium has a cell surface proteoglycan composed of keratan sulfate chains, which are easily accessible for immunolabeling.[1,20] A schematic diagram of this model system is shown in Figure 1. Critically, the corneal endothelial cells express cell surface keratan sulfate to different degrees, so some cells express very high levels, while others express such low levels they are undetectable with light microscopy. This differential labeling makes this model system ideal to determine the sensitivity of SERS.

RESULTS

The endothelial cells exhibited the characteristic differential expression of keratan sulfate, as previously reported.[1] Bright-field light microscopy results clearly show labeling for keratan sulfate on the surface of the endothelial cells (Figure 2A). Immunolabeled cells with a higher density of silver nanoparticles appear darker under light microscopy. Control samples show no labeling (Figure 2B). It is evident that the level of labeling varies from cell to cell. In extreme cases, adjacent cells vary between heavy labeling and levels that are undetectable by light microscopy, but can be detected using scanning electron microscopy.

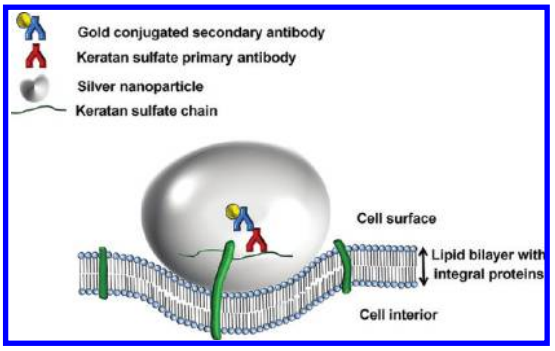

Figure 1. Schematic diagram of the immunolabeling process on the endothelial cell surface. The figure shows the primary antibody binding to keratan sulfate, the secondary antibody conjugated to 5 nm colloidal gold, and the silver nanoparticle.

SEM micrographs (Figure 2C) show antibody labeling to be uniform across individual cell surfaces. The silver nanoparticles appear bright under the electron beam (Figure 2C). The sensitivity of SEM is much higher than light microscopy, and under the SEM it is evident that even the cells that appear unlabeled with the light microscope do have some silver nanoparticles on their surface. Figure 2D shows a control corneal sample; no silver nanoparticles are present on the cell surface. Figure 2E shows a higher magnification of a labeled cell. Here, individual silver nanoparticles can be clearly resolved. High-resolution SEM shows that the nanoparticles are often in very close proximity to each other (Figure 2E inset). Figure 2F shows a histogram of the size distribution of silver nanoparticles. The average silver nanoparticle size was 227 nm. The highest density of silver nanoparticles found on a cell was 670 nanoparticles per 100 μm^2 and the lowest, 51 nanoparticles per 100 μm^2.

Spectra were acquired from cells with the highest density of silver nanoparticles, from cells with the lowest density of nanoparticles at 0.1% laser power, and from control samples at 0.1% and 100% power. Figure 3 shows median spectra from the highest density of labeling (blue), the lowest density of labeling (red), and unlabeled control cells (brown) at 0.1% laser power and unlabeled control cells at 100% power (pink). Wavenumbers of the enhanced peaks at 720, 850, 1320, and 1548 cm^{-1} are indicated. Figure 3 shows that no discernible spectrum was produced from the control cells when using 0.1% laser power. In contrast the spectrum from the silver nanoparticle-labeled cells showed

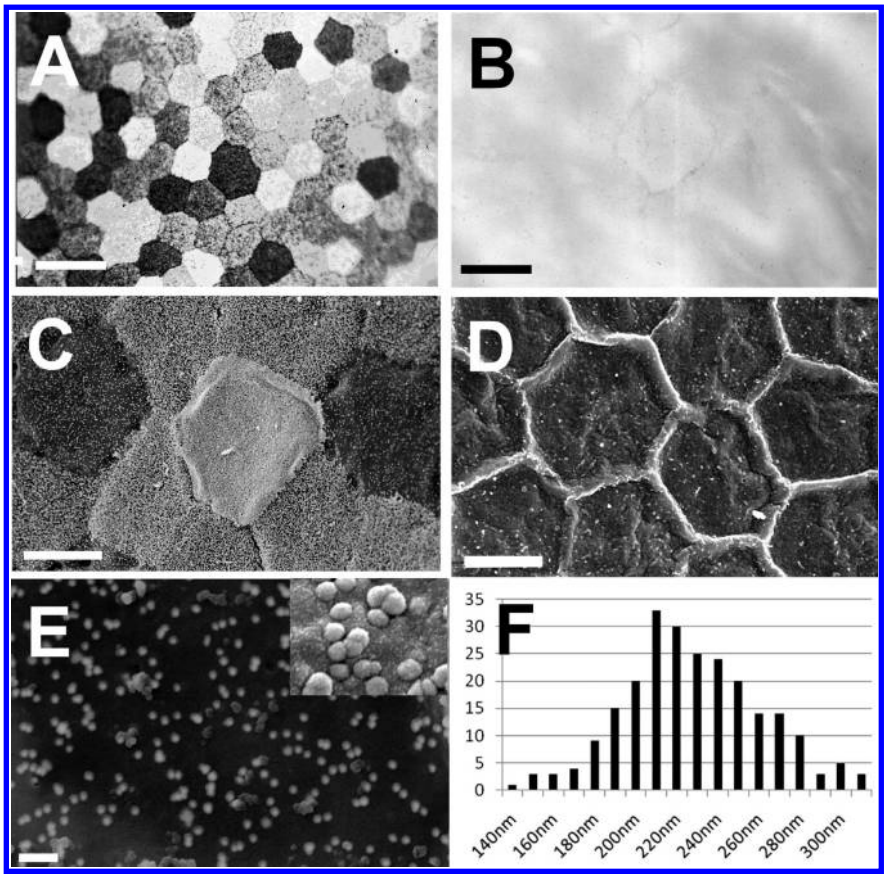

Figure 2. (A) Light micrograph of corneal endothelium immunolabeled for keratan sulfate. Labeled cells appear darker. There is a high degree of variability of labeling within the cell population. Scale bar = 25 μm. (B) The control shows no labeling. Scale bar = 25 μm. (C) Scanning electron micrographs of the apical surface of corneal endothelium immunolabeled for keratan sulfate. Labeled cells appear brighter. Scale bar = 10 μm. (D) The control shows no labeling on the endothelial cell surface. Scale bar = 10 μm. (E) The silver nanoparticles appear as bright white dots on the cell surface. Scale bar = 1 μm. The inset shows individual nanoparticles at 5× higher magnification. (F) Histogram showing the range of silver nanoparticle sizes.

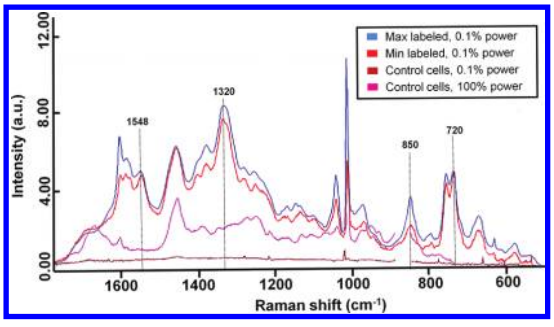

Figure 3. Median spectra from cells with the highest density of nanoparticles (blue), cells with the lowest density of nanoparticles (red), and unlabeled control endothelial cells (brown) all at 0.1% laser power. The pink trace shows unlabeled control cells at 100% power. Wavenumbers of the enhanced peaks at 720, 850, 1320, and 1548 cm^{-1} are labeled.

a large enhancement effect over the whole spectrum with a ~50-fold increase in signal at 1320 cm^{-1}.

The control cells (without nanoparticles) at 0.1% power produced no discernible spectra, but at 100% laser power a normal cell spectrum was produced. This spectrum was different from the silver nanoparticle enhanced cell membrane spectrum at 0.1% power (Figure 3).

Regions for spectral mapping were chosen on the basis of peaks that were enhanced in the presence of the silver nanoparticle and that did not appear in the control spectra.

Raman spectral imaging was performed by first carrying out a grid analysis, with data collection at uniform points within this grid. The grid covered several immunolabeled cells (Figure 4A). Once the data had been collected, several key wavenumbers were selected that had shown large enhancement effects and that did not appear on the control spectrum. The wavenumbers chosen were 720 cm^{-1} (Figure 4B), 850 cm^{-1} (Figure 4C), 1320 cm^{-1} (Figure 4D), and 1548 cm^{-1} (Figure 4E). These spectral maps all show an excellent correlation with the distribution of silver nanoparticles on the cell surfaces. Figure 4F shows a spectral map at 1320 cm^{-1} with a false color scale.

Figure 5 shows computational analysis of the spectral data with PCA and LDA. Figure 5A shows that 2D PCA-LDA produces a clear separation between the control and labeled cells; both maximum and minimum labeled cells are outside the 95% confidence control cluster. There is, however, overlap between the

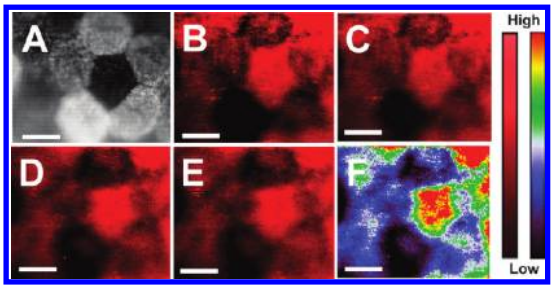

Figure 4. (A) Light micrograph of several corneal endothelial cells with varying densities of silver nanoparticles. The other figures show spectral mapping of these cells at wavenumbers as follows: (B) 720 cm^{-1}; (C) 850 cm^{-1}; (D) 1320 cm^{-1}; (E) 1548 cm^{-1}. (F) False spectral false color map at 1320 cm^{-1}. Scale bars = 20 μm.

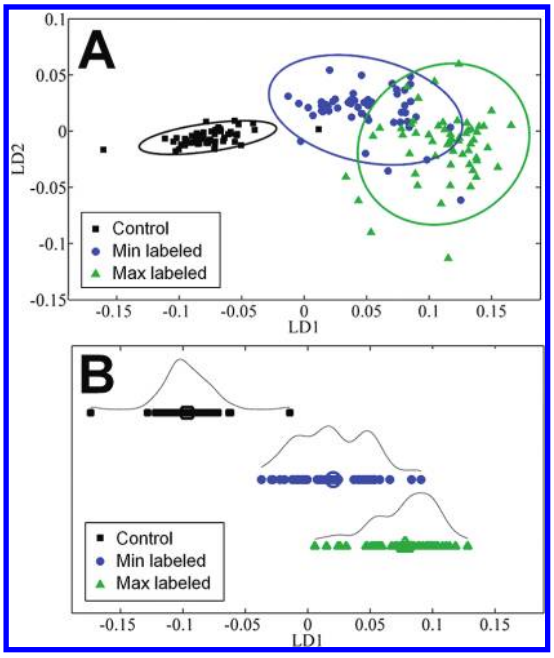

Figure 5. PCA and PCA-LDA of endothelial cell spectra obtained from cells with maximal nanoparticle density (triangles); cells with minimal nanoparticle density (circles); and unlabeled control cells (squares). (A) PCA-LDA 2D scores plot showing the distribution of the three data sets. A 95% confidence interval has been drawn around data classes. (B) PCA-LDA scores plot of the three data sets, along LD1.

minimum labeled cells and the maximum labeled cells. Figure 5B shows a 1D PCA-LDA scores plot of all three data sets; the control spectra show slight overlap with minimally labeled cells but no overlap with maximally labeled cells.

DISCUSSION

Our primary aim in this investigation was to determine if SERS biomolecular spectra could be obtained from the cell surface after using an immunolabeling protocol to attach silver nanoparticles to the cell membrane. Our results demonstrate that the silver nanoparticles produced a ~50-fold SERS enhancement effect. These spectra provide unique local biomolecular information from the cell surface.

The endothelial cell membrane is composed of a lipid bilayer made up of phospholipids with long fatty acid chains containing both saturated and unsaturated bonds. The basic structure of the cell membrane is a bilayer of phospholipids. Embedded within the lipid bilayer are numerous transmembrane proteins with hydrophobic alpha helical structures "dissolved" within the lipid bilayer itself. Also, present on the cell surface are glycol-lipids and glycoproteins. In this investigation we have concentrated our analysis on the peaks that are enhanced in the presence of the silver nanoparticles and that do not appear in the nanoparticle-free control spectra. We know that these enhanced peaks should be derived from the region adjacent to the silver nanoparticles;[19] this effectively means the cell membrane. Identification of peaks is not always definitive, as biological Raman is a relatively new field. However the Raman literature[21−29] shows that the enhanced peaks in our spectra are strongly associated with known cell membrane components (Table 1). For example the peak at ~720 cm^{-1} is associated with phospholipid heads. The peak at ~850 cm^{-1} covers a region associated with lipids, carbohydrates, and phospholipids. The peak at ~1320 cm^{-1} is probably derived from amide III associated with an alpha helical protein conformation; there is a broad area from ~1250 to 1400 cm^{-1}, which is a region associated with several different types of lipids. The peak at ~1450 cm^{-1} is also a lipid associated region, but as this peak is also present in the control, we speculate that it comes from lipid types present in both the membrane and cytoplasm. Finally, the peak at ~1548 cm^{-1} includes the amide II peak derived from alpha helical membrane proteins. Overall it is clear that the enhanced peak regions associated with membrane components and taken together provide evidence that the enhancement spectra are derived from their immediate environment local to the nanoparticles. There have been few previous experimental studies on how far the SERS enhancement effect is effective. However, a very useful paper by Tong and co-workers[19] has shown that most of the SERS enhancement effect of gold nanoparticles comes from within ~15 nm of the nanoparticle. The cell membrane is only some 9 nm thick, less than 1% of the overall cell thickness, and so would not normally be expected to make much contribution to a conventional Raman spectra. However, we show that by attaching silver nanoparticles to the membrane it is possible to obtain spectra information from this important and complex structure.

Supporting evidence comes from the spectral mapping of the enhanced peak wavenumbers. Spectral maps of the membrane component associated wavenumbers, 720, 850, 1320, and 1548 cm^{-1}, all show excellent correlation with the density of silver nanoparticles on the cell surface. The maps show a fairly even distribution of signal over the surface of the cell, as

TABLE 1. Raman Wavenumber Assignments Associated with Enhanced Spectral Peaks from Silver Nanoparticle Labeled Endothelial Cells

Raman peak wavenumber	biomolecular assignment	Raman peak wavenumber	biomolecular assignment
719 cm^{-1}	phosphatidycholine[23]	1308 cm^{-1}	lipid[22]
719 cm^{-1}	phospholipid head[21]	1313 cm^{-1}	lipid[21]
720 cm^{-1}	lipid[22]	1320 cm^{-1}	amide III[26]
733 cm^{-1}	phosphatidylserine[23]	1384 cm^{-1}	lipids[25]
840—70 cm^{-1}	glycolipid[24]	1440—55 cm^{-1}	saturated lipids[27]
865 cm^{-1}	phospholipid[24]	1446 cm^{-1}	lipid[21]
1254 cm^{-1}	lipids[25]	1450 cm^{-1}	phospholipid[28]
1266 cm^{-1}	lipids[25]	1452 cm^{-1}	lipid[22]
1270 cm^{-1}	fatty acids[23]	1548 cm^{-1}	amide II[25]
1295 cm^{-1}	lipids[25]		

would be expected with a cell membrane. However, by enhancing the signal contrast to its maximum by using false color imaging for wavenumber 1320 cm^{-1} we do see some evidence of a difference in intensity around the border of the labeled cell. This is in agreement with previous work that also obtained different Raman signal intensities from different regions of cells.[30] Cell membrane composition is known to be different at cell borders, and our findings reflect this

If we now look at the second objective of this paper, namely, to compare the sensitivity of SERS in the detection of nanoparticles relative to conventional light microscopy, the results are very interesting. It is clear that the SERS is able to detect silver nanoparticles *via* spectral enhancement at lower concentrations than is possible with conventional light microscopy, in fact, at levels comparable to that of electron microscopy. Electron microscopy has a very high level of sensitivity since the nanoparticles can be directly imaged, and in theory a single nanoparticle within a sample could be detected. However, electron microscopy is a very time-consuming technique, in both the preparation and examination of the samples. In addition, the preparation protocol can result in detrimental changes to the sample.[31] Thus, for the detection of immunolabeling, SERS offers a more sensitive alternative to light microscopy and a quicker and less destructive alternative to electron microscopy.

This paper shows that SERS is a remarkable technique both for the detection of immunolabeling and in providing unique spatially defined spectral information. The sensitivity of this technique can be partly attributed to the fact that we were able to maximize the SERS effect on the cell surface by using the optimum silver nanoparticle size and excitation wavelength.[15] We also speculate that the fact that many of the silver nanoparticles on the surface of our cells are in close proximity (Figure 2E inset) contributes to the SERS enhancement effect.[9,17]

CONCLUSIONS

This paper has demonstrated the usefulness and sensitivity of SERS when applied to cell surfaces labeled with silver nanoparticles. SERS has previously been used to detect antigens on a variety of cell types.[32—35] Other workers have used functionalized nanoparticles and SERS to image inside live embryos.[36] However, these workers have all used reporter molecules to enhance the SERS signal from the nanoparticles. The application of reporter molecules for SERS is reviewed by Matschulat and co-workers.[37] In contrast, in our study the nanoparticles are not modified by any reporter molecule. This means that although the sensitivity of this technique is far less than if a reporter molecule were used, the enhanced signal we are producing comes from the immediate environment around the nanoparticle, the endothelial cell membrane. Therefore the enhanced spectra contain novel information about the biomolecular composition of the cell membrane.

Overall, this investigation has shown that SERS spectra can be obtained from cells labeled using an immunogold-conjugated antibody to attach silver nanoparticles to the cell surface. The enhanced spectra provide unique biomolecular information from the cell membrane adjacent to the nanoparticles. Also, for the detection of nanoparticles SERS is more sensitive than conventional light microscopy and so has great potential in investigations where the concentration of epitope is too low to be detected with conventional methods.

MATERIALS AND METHODS

Specimens. Fresh bovine eyes, obtained from the local abattoir within 2 h of death, were transported to the laboratory on ice. On arrival, the corneas were immediately dissected out and fixed by immersion in 4% paraformaldehyde and 0.1% glutaraldehyde in phosphate-buffered saline (PBS) for a minimum of 30 min.

Antibodies. The monoclonal antibody (5-D-4) to the keratan sulfate glycosaminoglycan chain was obtained from ICN Biochemicals Ltd. (Thame, UK). The secondary was a goat anti-mouse IgG 5 nm gold-conjugated antibody (British Biocell International, UK).

Immunolabeling Procedure. After fixation, intact corneas were washed thoroughly in PBS buffer placed in 0.1 M glycine for

15 min and then washed again in PBS. The corneas were then incubated at room temperature with undiluted, normal goat serum for 20 min. The goat serum was then removed, and the corneal endothelium was incubated for 2 h at room temperature with the primary antibody at 1:100 dilution (5-D-4) in PBS buffer (pH 7.4) containing 1% bovine serum albumin (BSA) and 1% Tween 20. This was followed by a 30 min wash under agitation in two changes of the buffer. The samples were then incubated in the secondary antibody for 2 h at a dilution of 1:100 in PBS (pH 8.2) containing 0.5% BSA, 0.5% normal goat serum, 1% sodium chloride, 1% fish gelatin, and 1% Tween 20. This was followed by at least three 30-min washes in buffer alone, which was followed immediately by five 5-min washes in distilled water. For the control, the primary antibody was replaced by control mouse ascites fluid at an equivalent dilution.

Light Microscopy. The 5 nm colloidal gold particles were enhanced for light microscopy by the use of a silver enhancement kit (British Biocell International, UK). The enhancement procedure was performed for 15 min at room temperature. Corneas were then washed in distilled water, dehydrated through an alcohol series, and transferred to Histoclear before being mounted in DPX (Agar Scientific, UK), and photographed. Under the light microscope the immunolabeled cells appear dark, and unlabeled cells transparent. Samples had DPX removed by immersion in propylene oxide and then were air-dried. Samples were visualized by light microscopy prior to spectroscopy analysis.

Scanning Electron Microscopy. Immunolabeled samples were silver enhanced for 15 min, after which the samples were washed in distilled water and dehydrated through an ethanol series, then transferred to Peldri II or HMDS (Agar Scientific, UK), which was allowed to sublimate off. The samples were mounted on stubs and were sputter-coated with gold before being examined under a JEOL 840 SEM (JEOL, Tokyo, Japan).

Optimization of Nanoparticle Size. Nanoparticle size was influenced by the duration of the silver enhancement procedure. Enhancement for 15 min resulted in a mean nanoparticle size of 227 nm with a range of sizes between 140 and 320 nm.

Raman and Surface-Enhanced Raman Spectroscopy. Spectra were collected with a Renishaw inVia Raman microscope (Renishaw Inc., UK) with a 100 mW diode 785 nm laser. A 1200 lines/mm grating was used. The system was calibrated using the 520.5 cm^{-1} Raman band from a silicon wafer for wavenumber shifts. Fixed corneal samples were placed on MirrIR low-E glass slides (Kevley Technologies, USA), then visualized using bright-field microscopy to differentiate cells with a high density of silver nanoparticles from cells with a low level of silver nanoparticles. Raman spectra were collected in the range 400−2000 cm^{-1} using 0.1% and 100% laser power, 15 s exposure time, four accumulations, and a spot size of 1.2 μm^2 (Leica 50× objective, numerical aperture 0.75). The laser power at the sample was 38 mW/μm^2 using a 100% power setting and 0.038 mW/μm^2 for the 0.1% setting. The 100% setting was used only on cells with no silver nanoparticles. Data were collected and cosmic rays were removed using Renishaw Wire 3.1 (Renishaw Inc., UK). Spectra were baseline corrected using a rubber band algorithm[38] (OPUS, Bruker Optics Inc., USA) computed with 10 iterations and 64 points and vector normalized (OPUS, Bruker Optics Inc., USA). Small peaks at 853 and 875 cm^{-1} from ambient light were excluded from some spectra.

Raman Spectroscopic Imaging. Raman images were taken in a raster scan fashion using a Leica 50× objective (NA 0.75) and a 100 nm precision motorized stage (Renishaw Inc., UK) to position samples to the beam and a 830 lines/mm grating. SERS maps were collected overnight, generating several thousand spectra. SERS images were collected using 0.1% laser power and 5 s exposure time between the ranges 407−1260 $cm^{-1}$and 1250−2000 cm^{-1}. The step size was 0.6 μm. WiRE software was used to give a false color image of the collected data at a specific signal to baseline wavenumber.

Computational Analysis. To analyze our data sets of spectra and data points (wavenumbers), intricate algorithms for PCA or PCA-LDA were applied. We used MATLAB R2009 (TheMathsWorks, Natick, MA, USA) with a graphical user interface toolkit for spectroscopy (http://biophotonics.lancs.ac.uk/software) on the same spectral data sets used in Figure 3. Further software details are available in Patel *et al*., 2011.[39] PCA is an unsupervised data reduction technique producing a scores and loadings plot from derived principal components (PCs) of the mean-centered, processed spectra. Each PC was examined individually to determine which represented the best segregation of classes. Additional application of the supervised technique of LDA to the output process of PCA for the first 10 PCs was used (PCA-LDA). LDA maximizes the interclass variance in relation to the intraclass variance based on predefined class labels, giving optimal class segregation.[39] A scores plot was produced to visualize segregation of the classes, whereas derived cluster vector plots determined the wavenumbers responsible for segregation. Statistical significance of linear discriminants was carried out using 95% confidence intervals.

Acknowledgment. This work was supported by the Biotechnology and Biological Sciences Research Council, U.K.

REFERENCES AND NOTES

1. Fullwood, N. J.; Davies, Y.; Nieduszynski, I. A.; Marcyniuk, B.; Ridgway, A. E.; Quantock, A. J. Cell Surface-Associated Keratan Sulphate on Normal and Migrating Corneal Endothelium. *Invest. Ophthalmol. Vis. Sci.* **1996**, *37*, 1256–1270.
2. Herpers, B.; Xanthakis, D.; Rabouille, C. ISH-IEM: a Sensitive Method to Detect Endogenous mRNAs at the Ultrastructural Level. *Nat. Protoc.* **2010**, *5*, 678–687.
3. Chen, L.; Wei, H.; Guo, Y.; Cui, Z.; Zhang, Z.; Zhang, X. E. Gold Nanoparticle Enhanced Immuno-PCR for Ultrasensitive Detection of Hantaan Virus Nucleocapsid Protein. *J. Immunol. Methods* **2009**, *346*, 64–70.
4. Potučková, L.; Franko, F.; Bambousková, M.; Dráber, P. Rapid and Sensitive Detection of Cytokines using Functionalized Gold Nanoparticle-Based Immuno-PCR, Comparison with Immuno-PCR and ELISA. *J. Immunol. Methods* **2011**, *371*, 38–47.
5. Martin, F. L.; Kelly, J. G.; Llabjani, V.; Martin-Hirsch, P. L.; Patel, I. I.; Trevisan, J.; Fullwood, N. J.; Walsh, M. J. Distinguishing Cell Types or Populations Based on the Computational Analysis of Their Infrared Spectra. *Nat. Protoc.* **2010**, *5*, 1748–1760.
6. Martin, F. L.; Fullwood, N. J. Raman vs. Fourier Transform Spectroscopy in Diagnostic Medicine. *Proc. Natl. Acad. Sci. U. S. A.* **2007**, *104*, E1.
7. Fleischmann, M; Hendra, P. J.; McQuillan, A. J. Raman Spectra of Pyridine Adsorbed at a Silver Electrode. *Chem. Phys. Lett.* **1974**, *26*, 163–166.
8. Dieringer, J. A.; McFarland, A. D.; Shah, N. C.; Stuart, D. A.; Whitney, A. V.; Yonzon, C. R.; Young, M. A.; Zhang, X.; Van Duyne, R. P. Surface Enhanced Raman Spectroscopy: New Materials, Concepts, Characterization Tools, and Applications. *Faraday Discuss.* **2006**, *132*, 9–26.
9. Hafner, J. H.; Nordlander, P.; Weiss, P. S. Virtual Issue on Plasmonics. *ACS Nano* **2011**, *5*, 4245–4248.
10. Lee, S. Y.; Hung, L.; Lang, G. S.; Cornett, J. E.; Mayergoyz, I. D.; Rabin, O. Dispersion in the SERS Enhancement with Silver Nanocube Dimers. *ACS Nano* **2010**, *4*, 5763–5772.
11. Dadosh, T.; Sperling, J.; Bryant, G. W.; Breslow, R.; Shegai, T.; Dyshel, M.; Haran, G.; Bar-Joseph, I. Plasmonic Control of the Shape of the Raman Spectrum of a Single Molecule in a Silver Nanoparticle Dimer. *ACS Nano* **2009**, *3*, 1988–1994.
12. Xie, J.; Zhang, Q.; Lee, J. Y.; Wang, D. I. The Synthesis of SERS-Active Gold Nanoflower Tags for *in Vivo* Applications. *ACS Nano* **2008**, *2*, 2473–2480.
13. Chen, X.; Li, S.; Xue, C.; Banholzer, M. J.; Schatz, G. C.; Mirkin, C. A. Plasmonic Focusing in Rod-Sheath Heteronanostructures. *ACS Nano* **2009**, *3*, 87–92.
14. Shegai, T.; Brian, B.; Miljković, V. D.; Käll, M. Angular Distribution of Surface-Enhanced Raman Scattering from Individual Au Nanoparticle Aggregates. *ACS Nano* **2011**, *5*, 2036-2041.
15. Meyer, M. W.; Smith, E. A. Optimization of Silver Nanoparticles for Surface Enhanced Raman Spectroscopy of Structurally Diverse Analytes Using Visible and Near-Infrared Excitation. *Analyst* **2011**, *136*, 3542–3549.

16. Margueritat, J.; Gehan, H.; Grand, J.; Lévi, G.; Aubard, J.; Félidj, N.; Bouhelier, A.; Colas-Des-Francs, G.; Markey, L.; Marco De Lucas, C.; *et al*. Influence of the Number of Nanoparticles on the Enhancement Properties of Surface-Enhanced Raman Scattering Active Area: Sensitivity *versus* Repeatability. *ACS Nano* **2011**, *5*, 1630–1638.
17. Svedberg, F.; Li, Z.; Xu, H.; Käll, M. Creating Hot Nanoparticle Pairs for Surface-Enhanced Raman Spectroscopy Through Optical Manipulation. *Nano Lett.* **2006**, *6*, 2639–2641.
18. Nie, S.; Emory, S. R. Probing Single Molecules and Single Nanoparticles by Surface-Enhanced Raman Scattering. *Science* **1997**, *275*, 1102–1106.
19. Tong, L. M.; Li, Z. P.; Zhu, T.; Zhu, H.; Liu, Z. Single Gold-Nanoparticle-Enhanced Raman Scattering of Individual Single-Walled Carbon Nanotubes via Atomic Force Microscope Manipulation. *J. Phys. Chem. C* **2008**, *112*, 7119–7123.
20. Tai, G. H.; Nieduszynski, I. A.; Fullwood, N. J.; Huckerby, T. N. Human Corneal Keratan Sulphates. *J. Biol. Chem.* **1997**, *272*, 28227–28231.
21. Stone, N.; Kendall, C.; Shepherd, N.; Crow, P.; Barr, H. Near-Infrared Raman Spectroscopy for the Classification of Epithelial Pre-Cancers and Cancers. *J. Raman Spectrosc.* **2002**, *33*, 564–573.
22. Jess, P. R.; Smith, D. D.; Mazilu, M.; Dholakia, K.; Riches, A. C.; Herrington, C. S. Early Detection of Cervical Neoplasia by Raman Spectroscopy. *Int. J. Cancer* **2007**, *121*, 2723–2728.
23. Krafft, C.; Neudert, L.; Simat, T.; Salzer, R. Near Infrared Raman Spectra of Human Brain Lipids. *Spectrochim. Acta. Part A* **2005**, *61*, 1529–1535.
24. Wu, H.; Volponi, J. V.; Oliver, A. E.; Parikh, A. N.; Simmons, B. A.; Singh, S. In Vivo Lipidomics Using Single-Cell Raman Spectroscopy. *Proc. Natl. Acad. Sci. U. S. A.* **2011**, *108*, 3809–3814.
25. Willets, K. A. Surface-Enhanced Raman Scattering (SERS) for Probing Internal Cellular Structure and Dynamics. *Anal. Bioanal. Chem.* **2009**, *394*, 85–94.
26. Schuster, K. C.; Reese, I.; Urlaub, E.; Gapes, J. R.; Lendl, B. Multidimensional Information on the Chemical Composition of Single Bacterial Cells by Confocal Raman Microspectroscopy. *Anal. Chem.* **2000**, *72*, 5529–5534.
27. Jarvis, R. M.; Law., N.; Shadi, I. T.; O'Brien, P.; Lloyd, J. R.; Goodacre, R. Surface-Enhanced Raman Scattering from Intracellular and Extracellular Bacterial Locations. *Anal. Chem.* **2008**, *80*, 6741–6746.
28. Manno, D.; Filippo, E.; Fiore, R.; Serra, A.; Urso, E.; Rizzello, A.; Maffia, M. Monitoring Prion Protein Expression in Complex Biological Samples by SERS for Diagnostic Applications. *Nanotechnology* **2010**, *21*, 165502.
29. Kneipp, K.; Haka, A. S.; Kneipp, H.; Badizadegan, K.; Yoshizawa, N.; Boone, C.; Shafer-Peltier, K. E.; Motz, J. T.; Dasari, R. R.; Feld, M. S. Surface-Enhanced Raman Spectroscopy in Single Living Cells Using Gold Nanoparticles. *Appl. Spectrosc.* **2002**, *56*, 150–154.
30. Huang, J. Y.; Zong, C.; Xu, L. J.; Cui, Y.; Ren, B. Clean and Modified Substrates for Direct Detection of Living Cells by Surface-Enhanced Raman Spectroscopy. *Chem. Commun. (Cambridge, U. K.)* **2011**, *47*, 5738–5740.
31. Fullwood, N. J.; Meek, K.M. A Synchroton X-ray Study of the Changes Occurring in the Corneal Stroma during Processing for Electron Microscopy. *J. Microsc.* **1993**, *169*, 53–60.
32. Kim, J. H.; Kim, J. S.; Choi, H.; Lee, S. M.; Jun, B. H.; Yu, K. N.; Kuk, E.; Kim, Y. K.; Jeong, D. H.; Cho, M. H.; *et al*. Nanoparticle Probes with Surface Enhanced Raman Spectroscopic Tags for Cellular Cancer Targeting. *Anal. Chem.* **2006**, *78*, 6967–6973.
33. Park, H.; Lee, S.; Chen, L.; Lee, E. K.; Shin, S. Y.; Lee, Y. H.; Son, S. W.; Oh, C. H.; Song, J. M.; Kang, S. H.; *et al*. SERS Imaging of HER2-Overexpressed MCF7 Cells Using Antibody-Conjugated Gold Nanorods. *Phys. Chem. Chem. Phys.* **2009**, *14*, 7444–7449.
34. Nguyen, C. T.; Nguyen, J. T.; Rutledge, S.; Zhang, J.; Wang, C.; Walker, G. C. Detection of Chronic Lymphocytic Leukemia Cell Surface Markers Using Surface Enhanced Raman Scattering Gold Nanoparticles. *Cancer Lett.* **2010**, *292*, 91–97.
35. Kennedy, D. C.; Tay, L. L.; Lyn, R. K.; Rouleau, Y.; Hulse, J.; Pezacki, J. P. Nanoscale Aggregation of Cellular Beta2-Adrenergic Receptors Measured by Plasmonic Interactions of Functionalized Nanoparticles. *ACS Nano* **2009**, *3*, 2329–2339.
36. Wang, Y.; Seebald, J. L.; Szeto, D. P.; Irudayaraj, J. Biocompatibility and Biodistribution of Surface-Enhanced Raman Scattering Nanoprobes in Zebrafish Embryos: In Vivo and Multiplex Imaging. *ACS Nano* **2010**, *4*, 4039–4053.
37. Matschulat, A.; Drescher, D.; Kneipp, J. Surface-Enhanced Raman Scattering Hybrid Nanoprobe Multiplexing and Imaging in Biological Systems. *ACS Nano* **2010**, *4*, 3259–3269.
38. Pirzer, M.; Sawatzki, J. Method and Device for Correcting a Spectrum. U.S. Patent 7359815, 2008.
39. Patel, I. I.; Trevisan, J.; Singh, P. B.; Nicholson, C. M.; Krishnan, R. K. G.; Matanhelia, S. S.; Martin, F. L. Segregation of Human Prostate Tissues Classified High-Risk (UK) Versus Low-Risk (India) for Adenocarcinoma using Fourier Transform Infrared or Raman Microspectroscopy Coupled with Discriminant Analysis. *Anal. Bioanal. Chem.* **2011**, *401*, 969–982.